Unmanned Systems, Vol. 14, No. 1 (2026) 201–214
© World Scientific Publishing Company
DOI: 10.1142/S230138502550089X

UNMANNED SYSTEMS
https://www.worldscientific.com/worldscinet/us

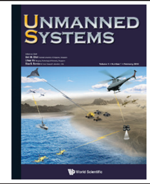

A Robust RANSAC Point Cloud Fitting Approach Based on the Bi-Objective Scoring Strategies

Fengling Li [*,‡], Zhengan Yin [*], Xiangqian Li [†], Junfeng Zhang [*]

[*]*College of Mechanical and Vehicle Engineering, Changsha, Hunan Province 410114, China*

[†]*Science and Technology Research Institute of China Three Gorges Corporation, Beijing 101100, China*

Laser scanning technology plays a pivotal role in diverse applications. However, challenges arise when fitting geometric point clouds or detecting objects using conventional RANSAC due to the dense concentration or uneven distribution of noise points along the boundaries of geometric objects. In this study, we propose a novel framework for random sample consensus (RANSAC) fitting, incorporating a bi-objective scoring function (BSFM). Initially, we introduce an innovative classification technique to optimize the accurate distinction between inliers and outliers within the geometry edge region. Subsequently, we construct a new bi-objective scoring function and iteratively optimize the model parameters of RANSAC, including error thresholds. To validate our method, comprehensive numerical tests are conducted under varying levels of noise pollution. The results demonstrate the superior performance of our approach compared to the three classical methods in terms of geometric fitting accuracy and robustness. Furthermore, when applied to the inspection of real reinforcing steel mesh, the evaluation indexes of our BSFM-RANSAC method surpass those of the conventional RANSAC technique.

Keywords: Geometric fitting; point cloud fitting; RANSAC; bi-objective scoring function.

1. Introduction

Point cloud data allow for the direct acquisition of precise spatial coordinates of the measured object, making it an essential tool in various applications such as engineering surveys [1] and intelligent driving perception tasks [2]. The ability to capture detailed 3D information has led to its widespread use in fields ranging from object recognition and feature extraction to 3D reconstruction and object segmentation. Geometric fitting based on laser point data is particularly vital in these research areas, serving as a foundational technology that enhances accuracy and efficiency in analyzing and interpreting spatial data.

Point cloud fitting is a complex process aimed at creating a mathematical model that accurately represents the characteristics and dimensions of the detected object [3]. In real-world scenarios, geometric fitting often suffers from low precision or false errors [4, 5], mainly due to noise interference in the point cloud, which distorts its morphological features. Additionally, the sparsity of 3D laser point cloud datasets complicates geometry fitting and object detection. Factors such as small object size, registration issues, and distortion further introduce uncertainties that challenge the accurate fitting of target geometry.

Over the past few decades, numerous point cloud fitting methods have been developed. Among the classical mathematical model methods, the least square method (LSQ) primarily focuses on optimizing the solution direction, but exhibits limited robustness against noisy data.

The RANSAC [6] (random sample consensus) algorithm, as demonstrated by Fischler *et al.*, has been proven to be an exceedingly robust fitting framework, even in the presence of a substantial number of outliers. RANSAC randomly selects a specific number of data points as the minimum sample set and then searches for the best fit by maximizing the number of inliers. The statistical framework of RANSAC is widely recognized for its effectiveness in distance data

Received 5 April 2024; Accepted 10 November 2024; Published 22 March 2025. This paper was recommended for publication in its revised form by editorial board member, Zhi Gao.
Email Address: ‡*003634@csust.edu.cn*
‡Corresponding author.

segmentation and robust model fitting, delivering superior results even when erroneous data (e.g. roughness) exceed 50% [7]. However, traditional RANSAC algorithms sample multiple times to achieve robustness, without efficiently utilizing data characteristics and historical information [4, 8].

Over the past few decades, research has primarily focused on three key factors that influence the accuracy of model fitting. The first crucial factor is the number of samples, which directly impacts the algorithm's computational speed and robustness, requiring a balance between accuracy and efficiency. RANSAC typically determines this value based on prior knowledge of the outlier percentage and the desired confidence level (e.g. 99%) to obtain an outlier-free model. When prior knowledge is unavailable, Chum [9] proposed stochastic RANSAC, which uses a sequential probability ratio test to achieve the same level of confidence. Additionally, Barath [10] introduced an adaptive sampling method in RANSAC, specifically tailored for image-matching problems.

The second influential factor is the error scale, which serves as a threshold to distinguish between inlier and outlier values. There are generally two different approaches to defining the boundaries. One approach is to select a fixed threshold based on prior knowledge or experience, such as the explicit value used in classical RANSAC. The other approach involves adaptively adjusting the error threshold at each iteration based on the residuals of the current inliers. For instance, MLESAC [11] dynamically adjusts the initial error threshold based on the percentage of data points classified as inliers. Chum *et al.* [9] focused on inliers with higher fitting accuracy in the early iterations by dynamically adjusting the error threshold, gradually relaxing it in later iterations to enhance robustness. ARRSAC [12] adjusts the error threshold dynamically based on the number of current inliers and the overall number of samples. Moisan *et al.* [13] proposed an opposite RANSAC approach, known as MinPRAN, which selects the most likely noise scale for each model. Additionally, Raguram–Heinrich introduced the SIMFIT algorithm, which efficiently and reliably performs both scale estimation and model estimation without a collapsing point.

The final key factor is the evaluation metric of the model, which is typically employed to assess the accuracy of the assumed model in the presence of contaminated data. For instance, the raw scoring function in RANSAC is based on the number of inliers that fit the model within a certain tolerance. MSAC [14] utilizes the minimization of the sum of residuals as an evaluation metric for simulation fitting. In MAPSAC [15], robust estimation is formulated as the estimation of data distribution parameters and the maximum *a posteriori* quality of the model. MINPRAN [16] assumes that outliers are uniformly distributed and seeks the model that is least likely to occur randomly internally. MAGSAC [15] incorporates the inherent uncertainty in threshold estimation by marginalizing the quality function over a range of noise levels. In the recently proposed MAGSAC++ [10], an iterative reweighted least squares optimization algorithm is introduced, which calculates weights for the best model based on the probabilities of inliers.

In the aforementioned studies, the majority of noise values in point cloud datasets are either uniformly distributed or located significantly away from the target point cloud. Consequently, it is essential to identify a model that minimizes the occurrence of internal outliers and enhances fitting accuracy by utilizing a fixed threshold and maximizing the internal point evaluation index. However, there is a need for further exploration to address the challenge of inadequate fitting accuracy caused by excessive noise data at the geometric edges. Therefore, this paper focuses on addressing the issue of insufficient fitting accuracy in geometry detection using RANSAC, specifically due to the presence of excessive noise data at the geometric edges. The following contributions are made:

(1) This paper introduces a novel adaptive error threshold fitting method, named BSFM-RANSAC, which extends the existing RANSAC framework. BSFM-RANSAC effectively addresses the issue of excessive geometric size error resulting from the presence of excessive noise at the geometric edge.
(2) The proposed BSFM-RANSAC method introduces a novel classification technique for distinguishing between inliers and outliers, thereby enhancing the decision-making process for points on the edge of geometry.
(3) A novel model evaluation index is proposed, accompanied by the introduction of a double objective scoring function. These modifications aim to optimize the evaluation criteria in the original RANSAC algorithm by utilizing a single point-based approach.

We organize the rest of this paper as follows: In Sec. 2, we introduce the method of consistency sampling. In Sec. 3, we introduce the objective function and arithmetic procedure of this optimization algorithm. In Sec. 4, we use this algorithm for model fitting of synthetic and real data, and we prove the truthfulness and effectiveness of the algorithm through experiments. In Sec. 5, we summarize the proposed algorithm.

2. The RANSAC Method

2.1. *The proposed RANSAC framework*

The RANSAC algorithm aims to ensure that the points selected from the minimum sample set exclude all outliers with a certain confidence probability. The number of iterations, denoted as m, in the RANSAC algorithm can be theoretically estimated, and the loop termination condition should satisfy the following criteria [2]:

$$m \geq \frac{\log(1-P)}{\log(1-\omega^n)}, \tag{1}$$

where n represents the minimum number of data points required to calculate the model parameters. The symbol ω denotes the probability of an inlier within the dataset, while P refers to the confidence level, typically set within the range of 95% to 99%.

The RANSAC algorithm, however, exhibits two limitations in its model evaluation technique. First, the algorithm's fitting accuracy is overly reliant on the details of the original data. Setting a high threshold value can result in a decrease in the accuracy of parameter estimation, while a small threshold value leads to a high rejection rate of the original data, thereby reducing the applicability of parameter estimation. Second, the sole criterion for assessing the quality of the model is the number of inliers based on the maximum set of hypotheses. Greedily selecting the model with the maximum number of inliers can lead to the problem of distorted model fitting.

The proposed method introduces a fitting accuracy optimization technique based on a bi-objective scoring function. This approach improves upon the original algorithm by replacing internal counts with new metrics that adjust the objective function of the evaluation criteria. The design framework, illustrated in Fig. 1, is divided into two phases: hypothesis generation and hypothesis evaluation.

In the hypothesis generation phase, the algorithm retains the original sampling randomness, randomly selecting the minimum number of samples and calculating the corresponding model parameters. During the hypothesis evaluation phase, the algorithm begins with a large initial threshold. Using a novel soft decision-making approach for inlier-outlier classification, objective function values are computed for the model as the threshold gradually increases. The bi-objective scoring mechanism identifies the inlier set with the highest quality score. This process is repeated over multiple iterations, terminating after m iterations. The scores from the best inlier set are then used to determine the optimal model parameters and thresholds.

3. BSFM-RANSAC Method

3.1. *Concentration function*

In this paper, the set of input data points is represented as $P = \{p | p \in R^v, v \in N > 0\}$, where v denotes the dimensionality of the points. For example, when $v = 2$, P represents a set of two-dimensional points, and when $v = 3$, P represents a set of three-dimensional points. The model being fitted is denoted by its parameter vector θ, where $\theta = \theta | \theta \in R^u, u \in N > 0$, and u represents the number of model parameters. In this section, the concentration function S_c [7], introduced by Torr and Zisserman, is utilized as the objective function for iterative optimization. Particularly in the inlier-outlier decision-making process, a flexible curve is employed to transition from a hard decision, based solely on an error threshold (binary: 0 or 1), to a soft decision. This soft decision-making approach optimizes the classification of inliers and outliers in the geometric edge region. The objective concentration function score Sc is formulated as follows:

$$S_c(\theta, P) = \frac{\sum_{i=1}^{N} f_v(R(\theta, p), \delta)}{N - S}, \tag{2}$$

where the function R denotes the residual function, N denotes the total number of datasets, δ denotes the error threshold, S denotes the minimum number of sample points required to fit the model, not using Boolean variables $(0\ or 1)$ to compute the degree of inliers of the data points around the error scale δ, where the function f_v is defined

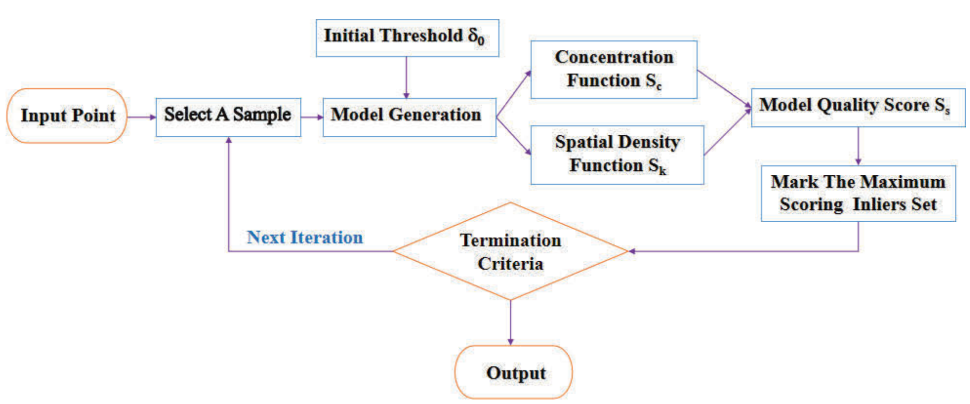

Fig. 1. The BSFM-RANSAC algorithm framework.

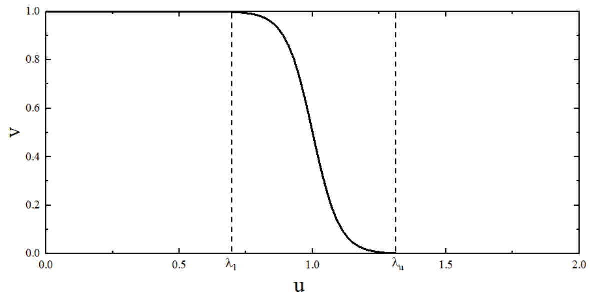

Fig. 2. Inliers/outliers classification curve.

as follows:

$$f_v(u) = \begin{cases} 1 & \text{for } u \le \lambda_1, \\ g(u) & \text{for } \lambda_1 \le u \le \lambda_u, \\ 0 & \text{for } u \ge \lambda_u, \end{cases} \tag{3}$$

where $u = R(\theta, p)/\delta$ denotes the normalized residuals, and the function $g(u)$ is a logistic Steele classification function 4. It uses a flexible curve to determine the degree of the inliers of the data points in the Geometric Edge Region, which mitigates the sensitivity of the original algorithm's hard decision-making based on the error threshold for describing the smooth transitions in this region, and the parameters λ_1 and λ_u determine the lower and upper bounds of the flexible region, and we have set $(\lambda_1, \lambda_u) = (0.7, 1.3)$, and the related support functions are shown in Fig. 2. The geometric edge region refers to areas within the point cloud where the boundary between inliers (points that conform to the model) and outliers (points that do not conform to the model) is not clearly defined. These regions often occur near the edges or transitions of geometric shapes, where noise or measurement errors make it challenging to distinguish between points that belong to the model and those that do not. In such regions, a hard decision-making approach based solely on a fixed error threshold may misclassify inliers as outliers or vice versa. By using a flexible curve, our method allows for a gradual transition between inliers and outliers, improving the classification accuracy in these ambiguous regions. The parameters were selected based on empirical observations that suggest these values provide a balanced trade-off between flexibility and stability in the classification process.

$$P(x) = \frac{1}{1 + e^{\frac{x-\mu}{s}}}, \tag{4}$$

where μ and s are constants representing the positional and shape parameters, respectively.

3.2. *Spatial density function*

The original RANSAC algorithm evaluates model quality solely based on identifying the model with the highest number of inliers within a given *inlier/outlier* threshold. However, this approach overlooks the actual spatial geometric characteristics of the target. In practical engineering applications, finding the optimal target model and its parameters can be challenging. This phenomenon can be illustrated through a simple example, as shown in Fig. 3. When the error threshold is set to L_2 and $L_2 > L_1$, both Line 1 and Line 2 can emerge as hypotheses in the algorithm with an equal number of inliers. Consequently, either line can be considered as the optimal solution. However, it is evident that the geometry of Line 1 is superior to that of Line 2. To address this limitation, this section introduces a novel model evaluation metric called the spatial density score S_k. This metric represents the sparseness of the inlier distribution in the model. The higher the value of this function, the tighter the distribution of inliers around the model, indicating a more proportional geometry and higher quality.

$$S_k(\theta, p) = \frac{jS_c(\theta, p)}{V_\theta}, \tag{5}$$

where j is a constant, S_c denotes the point concentration function within the model, and V_θ denotes the volume occupied by the target model space.

3.3. *Quality scoring function*

A tangled issue in geometric model fitting is whether the data points should be clustered based on the number of

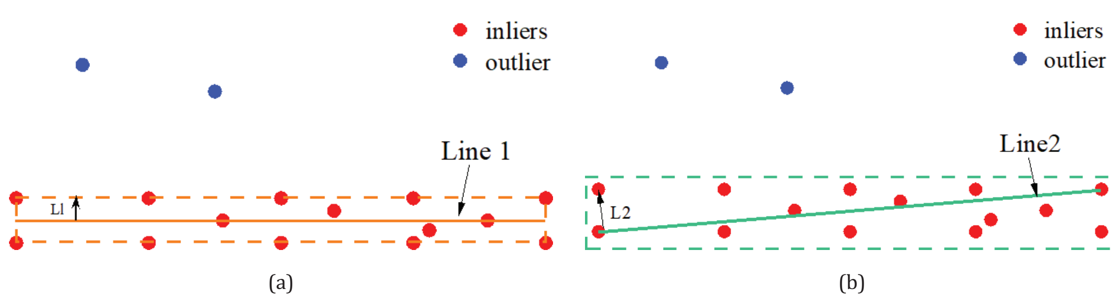

Fig. 3. Illustration of spatial density function of point cloud (a) ideal model Line 1 (b) interference model Line 2.

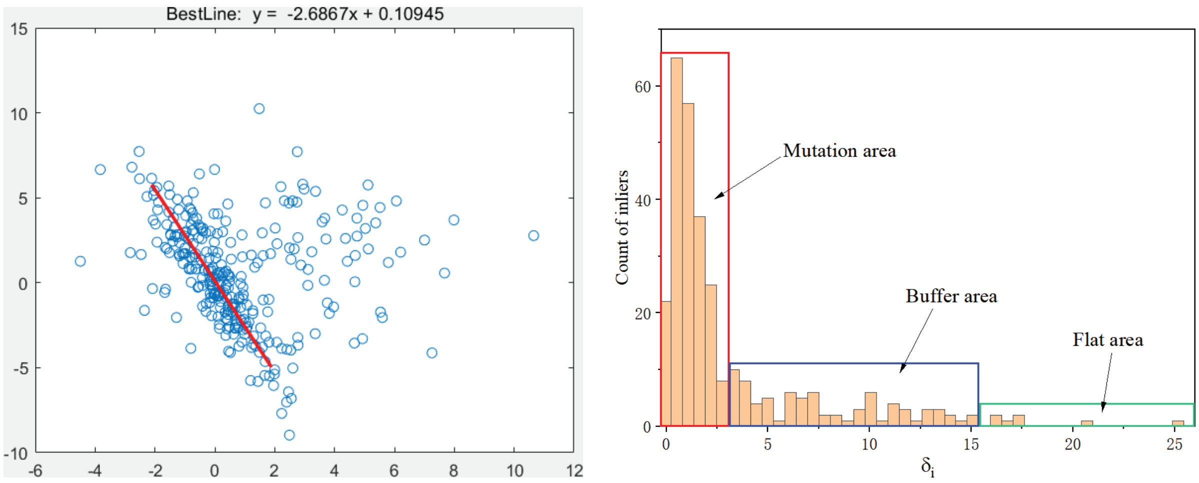

(a) (b)

Fig. 4. Illustration of the quality scoring function (a) Point cloud image with noises; (b) Concentration distribution of inliers in each residual interval.

inliers in the model or based on the geometric proximity of the model. If the threshold is taken to be too small, it will make the number of points within the model too small and result in shapes that are difficult to form, and if the threshold is too large, it will cause excessive geometric errors caused by too many points that do not originate from the model being sought. In order to balance the two, we try to find the boundary point that maximizes the density of inliers while also minimizing the error threshold. Taking the histogram of the two-dimensional linear residual distribution (Fig. 4) as an example, we believe that certain thresholds $(\delta_1, \delta_2, \ldots, \delta_n) < \delta_{\max}$ exist, which make a significant mutation in the concentration of the inliers, and we consider that this boundary point is most likely to appear at the point where the local concentration gradient of the inliers changes most significantly, and we collectively refer to these mutation significant points as the "nominal thresholds". In this paper, we find the optimal model by calculating the quality scores of the models corresponding to different nominal thresholds during the iteration process. The formula for calculating the quality score is as follows:

$$S_s(\theta, \delta, P) = \left[\left[\frac{|b_i - b_{i+1}|}{b_i} > \alpha\right]\right][\beta S_c(\theta, p) + (1-\beta)S_k], \tag{6}$$

where S_c denotes the concentration function, S_k denotes the spatial density function, α denotes the mutation significant coefficient, $0 < \alpha < 1$, β denotes the scoring weights, which depend on the application, and $[[.]]$ is the Iverson bracket, which is one if the internal condition holds, and zero otherwise. It is worth mentioning that, the S_s quality scoring function cannot increase monotonically with the number of inliers, otherwise $\delta_{\max}$ will always be the maximum value.

3.4. *Determination of optimal threshold*

The initial fit in this paper is done with a fairly large error threshold $\delta_{\max}$, and divided into n intervals as shown in Fig. 4, and from the smallest samples within the RANSAC, the concentration of the inliers in the neighboring residual thresholds is calculated with the following formula:

$$b_i = \frac{1}{N}\left[\left[\frac{i\delta_{\max}}{n} \le R(p, \theta) \le \frac{(i+1)\delta_{\max}}{n}\right]\right], \tag{7}$$

where N denotes the total number of datasets and the function R denotes the residual function, $i \in [0, n)$. We assume that the maximum threshold $\delta_{\max}$ is wide enough to accommodate the optimal threshold δ_{best}, i.e. $0 \le \delta_{\text{best}} \le \delta_{\max}$. We determine the optimal threshold for the optimal model by using the error threshold associated with the highest-rated hypothetical model, as given by the following formula:

$$\delta_{\text{best}} = \operatorname{argmax} S_s(\theta, \delta_i, P), \tag{8}$$

where the function q denotes the model parameters, $0 \le \delta_i \le \delta_{\max}$.

4. Experiments

To verify the correctness and effectiveness of the algorithm, we conducted performance tests on both synthetic and real datasets, comparing the optimization algorithm with similar

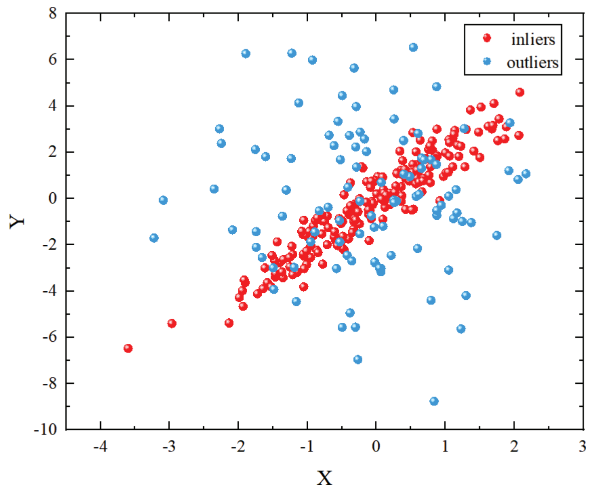

Fig. 5. Original image.

approaches. Firstly, we performed simulations of two-dimensional straight line fitting using synthetic datasets. This step aimed to confirm the feasibility of the algorithm under controlled conditions. Subsequently, we conducted experimental comparisons and accuracy assessments using a real steel mesh dataset obtained through LIDAR scanning. The dataset contains three-dimensional straight line characteristics. This evaluation aimed to validate the algorithm's real-world effectiveness and superiority compared to other methods.The data acquisition equipment for the steel mesh in the field is the CH32 series intelligent LiDAR (32-line hybrid solid-state laser radar) by Lei-Shen. The horizontal angle resolution of the LiDAR used varies with the scanning speed. After several experiments, it was found that the optimal point cloud collection time and data distortion rate occur when the scanning speed is set at 10 Hz.

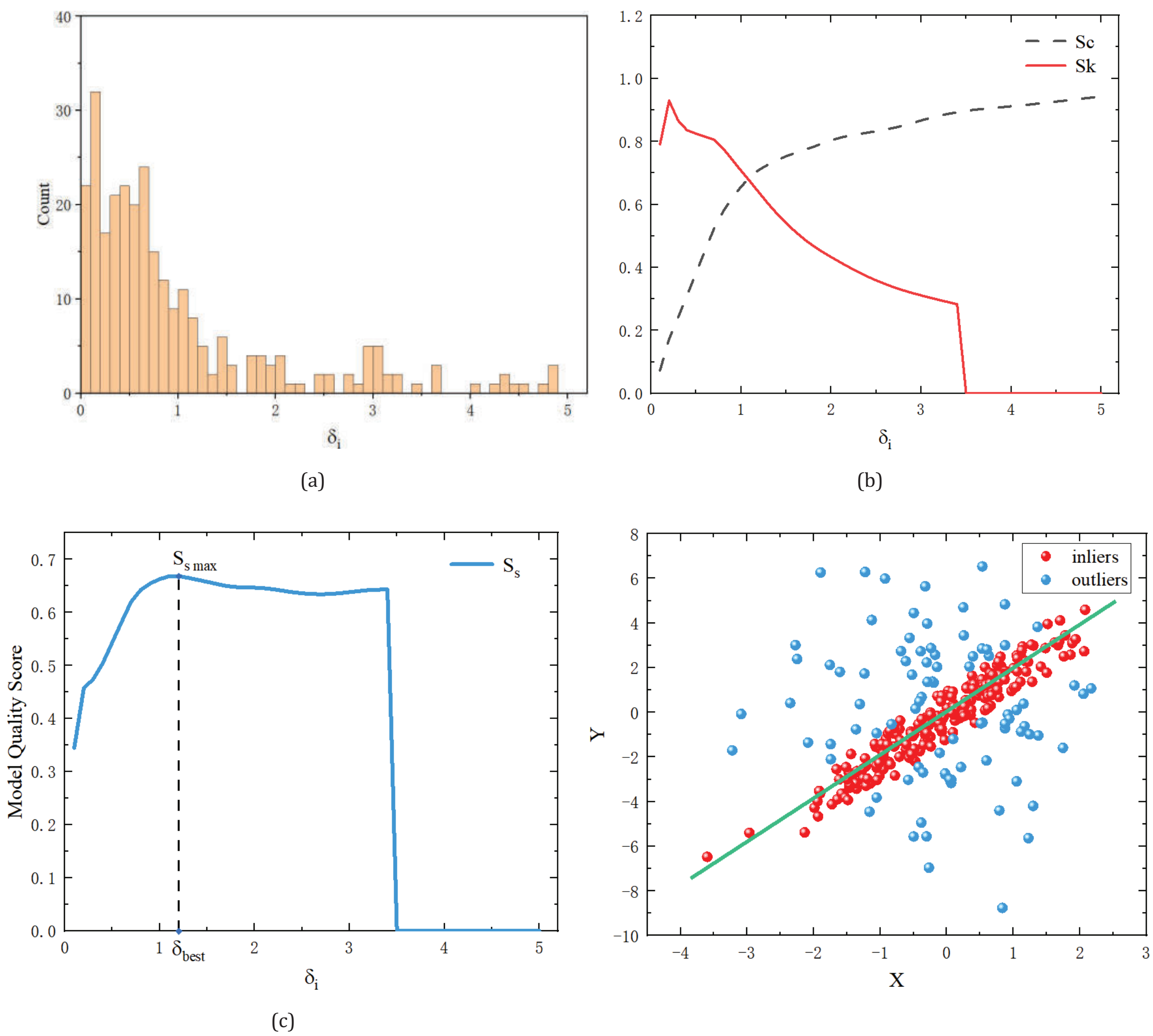

Fig. 6. (a) Residual-numbuer of inliers distribution histogram; (b) inliers concentration function and spatial density function; (c) model quality rating function and (d) result using BSFM-RANSAC.

4.1. *2D experiments*

4.1.1. *2D line simulation experiment*

In order to improve the detection difficulty, the synthesized data D consisted of 200 inliers D_1 obeying Gaussian distribution and 100 random noise (outliers) D_2, which was used as the original input image for this experiment, as shown in Fig. 5.

The optimization algorithm follows a specific procedure. Initially, two points are randomly selected from a pool of 300 candidate points using the RANSAC sampling strategy. These points serve as the primary sample set for model fitting. Next, a provisional model is derived using a relatively large error threshold. The given error threshold is divided into 50 intervals. In each interval, the inlier density is computed for the assumed model with progressively increasing residuals. To assess the quality of the models, two metrics are incorporated: the inlier concentration score S_c and the spatial density score S_k corresponding to the nominal threshold. These metrics provide measures of the concentration of inliers and the sparseness of their distribution around the model, respectively. A weighted sum of these two metrics is used to calculate the comprehensive model score. The model with the highest score, determined through this evaluation process, is designated as the optimal model for that iteration. The corresponding threshold for this model was considered the best threshold. The quality score S_s for the model was derived using Eq. (6). After m iterations, as derived from Eq. (1), the scores of the optimal models from each iteration were compared. The model with the paramount score was finalized as the best-fit model, showcased in Fig. 6(d).

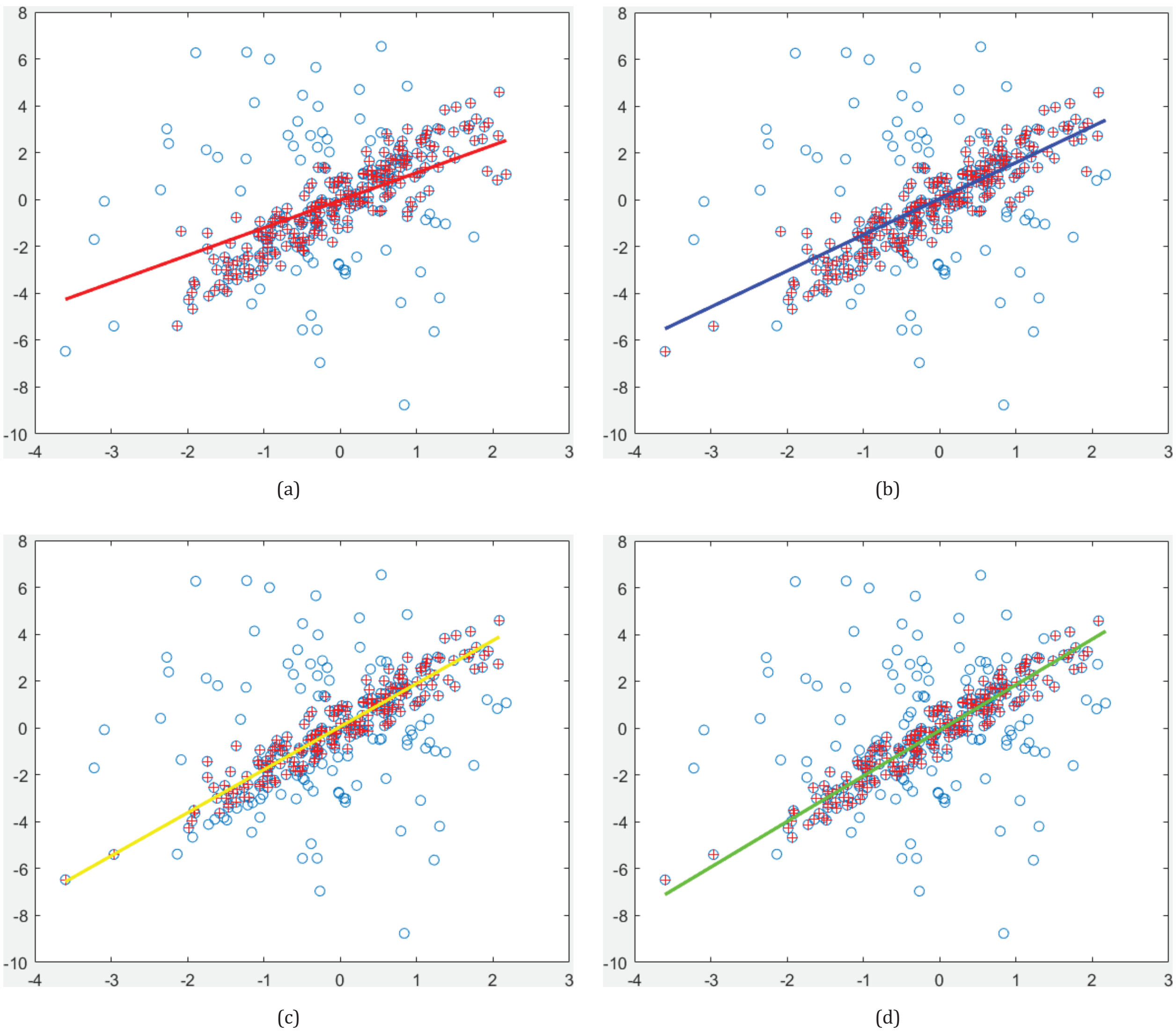

Fig. 7. Resulits in different algorithms. (a) Least squares fit, (b) RANSAC, (c) MSAC and (d) BSFM-RANSA.

Table 1. Evaluation of the correct matching rate of inliers and the fitting accuracy for 10 trials.

Algorithm	Mean number of inliers	Mean inliers matches	$A(\hat{P})$	$A(\hat{k})$	Fitting accuracy
LSQ	227	184	81.06%	1.1750	59.69%
RANSAC	**240**	**197**	82.08%	1.5435	78.41%
MSAC	207	177	85.51%	1.8386	93.40%
BSFM-RANSAC	213	185	**86.85%**	**1.9486**	**98.98%**

Note: Best results are highlighted in **bold**.

Given that D_1 represents a known linear model in the synthesized data, the slope K can be calculated using the least squares method in the absence of interference. In order to determine the error thresholds required by the RANSAC and MSAC algorithms, we consider the maximum residuals from the straight line in the inlier set D_1 as the theoretically optimal error threshold. This threshold is computed to be 1.9686. Subsequently, we performed straight-line fitting using the LSQ, RANSAC, MSAC, and BSFM-RANSAC algorithms. We set the number of iterations to 2000 to ensure sufficient exploration of the solution space. To minimize the influence of experimental chance, each algorithm was executed 10 times, and the final experimental results were averaged. The fitting results are presented in Fig. 7.

In this section, we express the correct matching rate of inliers as the correct rate of the algorithm's object detection in noisy environments, and the calculation of the slope K value reacts to the accuracy of the algorithm's parameter estimation, the average interior point matching rate $A(\hat{P})$ and the average estimated slope $A(\hat{k})$ are calculated as follows:

$$A(\hat{P}) = \frac{1}{S}\sum_{i=1}^{S} |\hat{P}_i|, \tag{9}$$

and

$$A(\hat{K}) = \frac{1}{S}\sum_{i=1}^{S} |\hat{K}_i|, \tag{10}$$

where $\hat{P}_i$ and $\hat{K}_i$ are the estimated inlier matching rate and the slope of the straight line for the ith sample, respectively, while S is the number of experimental runs, which is set to 10 here. As indicated in Table 1, the proposed optimization algorithm in this paper outperforms the other three algorithms in terms of the matching rate of interior points and the accuracy of parameter estimation.

RANSAC is widely recognized as a robust model estimation method that performs well in datasets contaminated with up to 50% noise. However, we argue that it has inherent limitations when dealing with high-noise scenarios. As the noise level increases, there is a possibility that certain random models may contain more inliers than the true model. To investigate this, we conducted interference tests using the inlier dataset D1 obtained from the previous section, along with synthetic datasets containing varying levels of noise. Four fitting algorithms were subjected to these tests, as illustrated in Fig. 8.

Comparing the experimental results presented in Table 2, it can be observed that the RANSAC algorithm demonstrates relatively good fitting performance in environments with noise levels of 50% or less. However, as the noise level exceeds 50%, the fitting results become significantly distorted. On the other hand, both the MSAC algorithm and the proposed BSFM-RANSAC algorithm in this paper exhibit better fitting accuracy overall. The optimization algorithm proposed in this paper outperforms the MSAC algorithm in terms of fitting accuracy, despite the increased computational cost. Moreover, there is no need

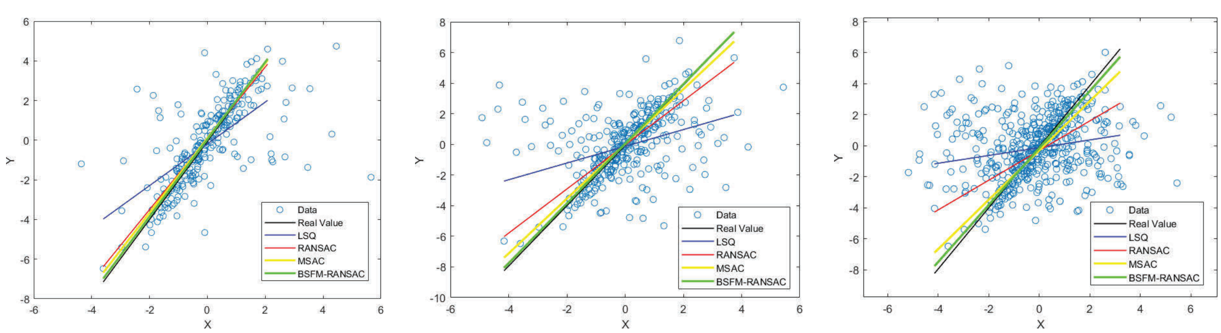

(a) (b) (c)

Fig. 8. Fitting results of different algorithms under different noise levels. (a) 20% noise. (b) 40% noise. (c) 60% noise.

Table 2. Evaluation of fitting accuracy under different noise levels.

Algorithm	Meas.	Added Noise level ϵ 20%	30%	40%	50%	60%	70%	Mean $\overline{\epsilon}$	Auto τ	Time t	Ξ
LSQ	Err.(m)	0.915	1.303	1.423	1.599	1.718	1.715	1.445	**Yes**	**0.14**	4.94
	Acc(%)	53.5%	33.83%	27.73%	18.77%	12.73%	12.87%	26.57%			
RANSAC	Err.(m)	0.170	0.486	0.528	0.831	1.013	1.551	0.763	No	0.79	1.65
	Acc(%)	91.3%	75.30%	73.16%	57.81%	48.55%	21.20%	61.23%			
MSAC	Err.(m)	<u>0.084</u>	<u>0.125</u>	<u>0.182</u>	<u>0.310</u>	<u>0.380</u>	<u>0.515</u>	<u>0.265</u>	No	<u>0.56</u>	<u>6.71</u>
	Acc(%)	<u>95.8%</u>	<u>93.64%</u>	<u>90.76%</u>	<u>84.27%</u>	<u>80.70%</u>	<u>73.83%</u>	<u>86.49%</u>			
BSFM.	Err.(m)	**0.011**	**0.050**	**0.075**	**0.122**	**0.158**	**0.246**	**0.110**	**Yes**	0.81	**11.19**
	Acc(%)	**99.5%**	**97.44%**	**96.20%**	**93.79%**	**92.00%**	**87.51%**	**94.40%**			

Notes: Best results are highlighted in **bold**, and second best in <u>underline</u>. τ indicates whether a manual threshold is required. Ξ is the scoring metric that reflects combined performance considering accuracy, time, and automation. $\Xi = \frac{\exp(\tau)}{\overline{\epsilon} \times t}$. The larger the value, the better it is.

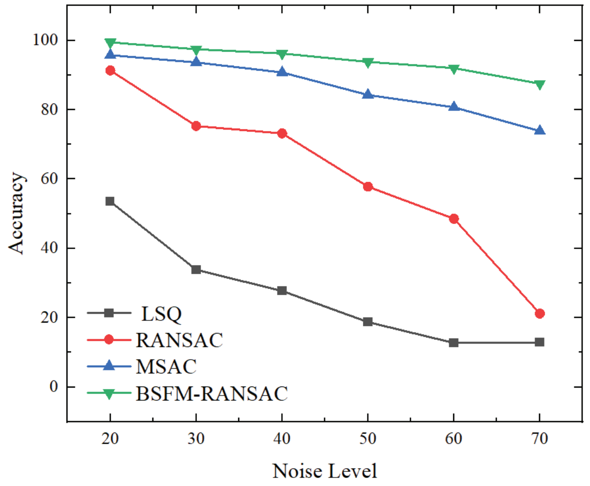

Fig. 9. The fitting accuracy of four algorithms under different noise levels.

for manual input of the maximum error threshold in advance, which significantly reduces the manual debugging effort and simplifies the process, making it more efficient.

The results of the algorithm accuracy comparison are shown in Fig. 9.

4.2. *Example analysis of real rebar structure*

To further substantiate the reliability and practicality of the algorithm proposed in this study, we conducted a precision evaluation of the geometric dimensions on a real-life rebar mesh. In this work, we only focus on the prefabrication rebar that is modularized and standardized. The rebar mesh, as shown in Fig. 10(a), consists of 14 rebars of similar geometric sizes: 7 positioned horizontally and 7 vertically. Each rebar has a radius of 0.036000.00050 m. These rebars are placed horizontally such that the vertical rebars form a 90 angle with the ground and the horizontal rebars are perpendicular to the vertical plane. After undergoing preprocessing steps such as pass-through filtering and plane removal, the resulting point cloud image can be seen in Fig. 10(c), comprising a total of 4,906 data points.

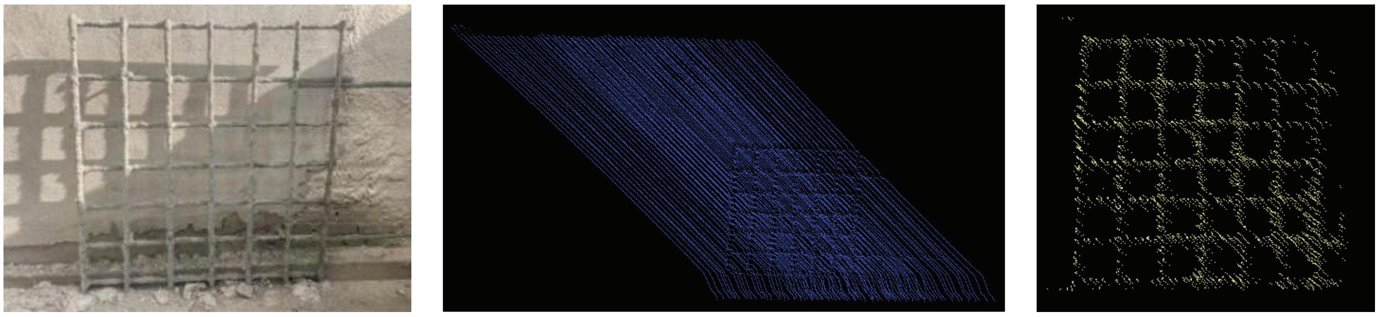

(a) (b) (c)

Fig. 10. (a) Original image of steel bars. (b) Original point cloud image. (c) Point cloud image after preprocessing.

Table 3. Comparison of accuracy of line plane angle.

Algorithm	Method	$A(\hat{Z})$	$\mathrm{MSE}(\hat{Z})$
Rebar1	RANSAC	88.079	3.690
Rebar1	BSFM-RANSAC	89.857	0.021
Rebar2	RANSAC	88.235	3.115
Rebar2	BSFM-RANSAC	89.616	0.134

4.3. *Ablation study*

The proposed solution consistently demonstrates higher accuracy in the presence of noise added to the scanned rebar data, as shown in Table 2. To simulate noise, we randomly altered a portion of the point positions. The results indicate that most state-of-the-art (SOTA) methods struggle to maintain accuracy under these conditions, with their performance declining rapidly as noise increases. In contrast, our method sustains high accuracy without the need for manually tuned thresholds.

However, it is important to note that while our method excels in accuracy, it is not the fastest in terms of raw processing time. Some less accurate methods are significantly faster. To address this trade-off, we propose a new scoring metric that combines accuracy, processing time, and the level of automation. This comprehensive metric reveals that our method outperforms others, highlighting its user-friendliness, accuracy, and ability to operate with minimal human intervention.

4.3.1. *Straight line fitting of a single steel bar*

The point cloud of a single rebar surface in a reinforcing mesh lacks structural information consistent with the shape semantics. Typically, RANSAC line estimation is employed to tackle the detection and localization of rebars [17]. However, RANSAC line detection on this raw dataset is particularly challenging due to several reasons: (1) the small radius of the rebars and the sparse point cloud on the rebar surface, (2) the rebar surface is mostly encapsulated by concrete, and the overall distribution of the point cloud is heavily disturbed by outliers, which makes it difficult to estimate the accurate straight line parameters, and (3) the

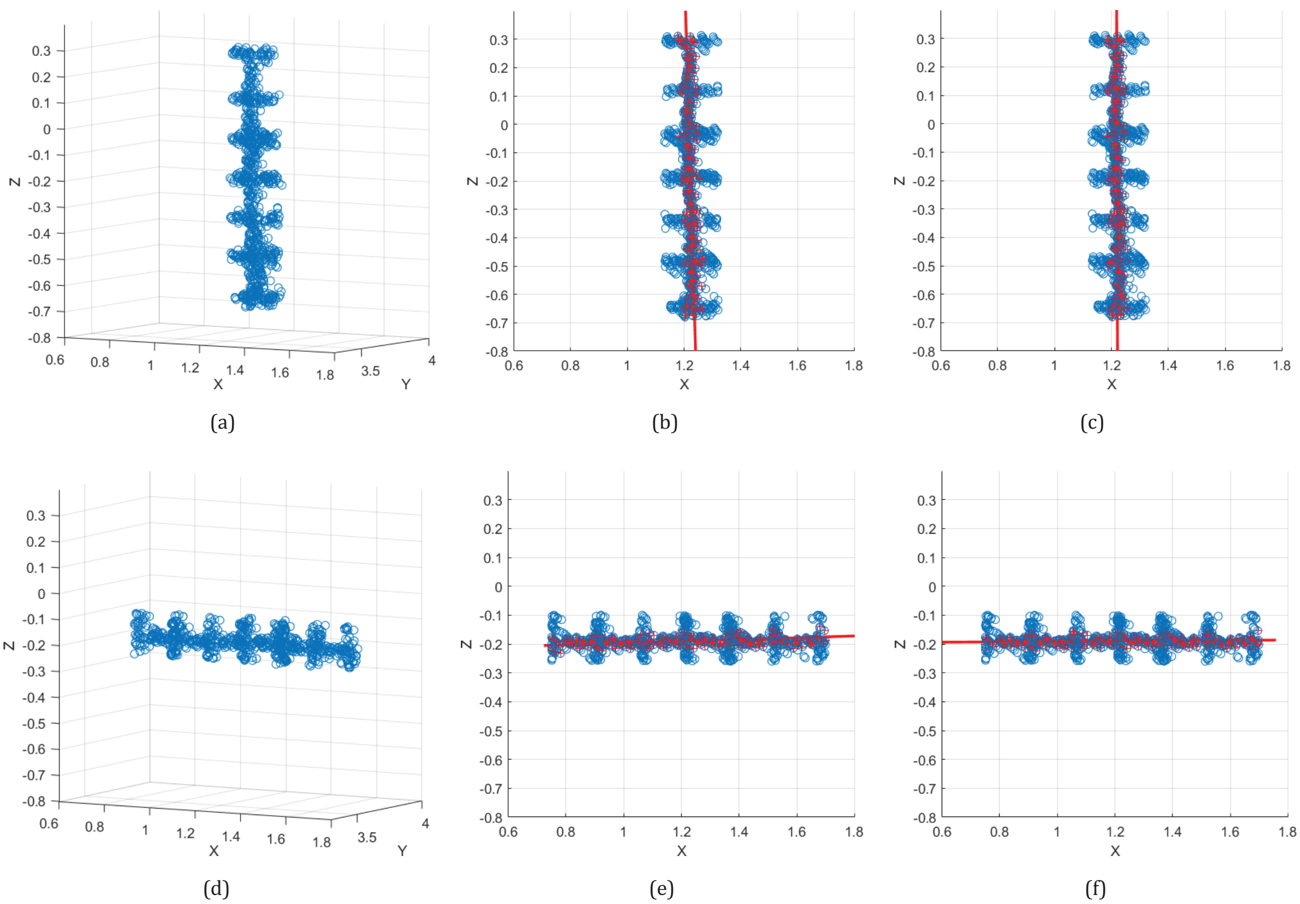

Fig. 11. (a)(d) Horizontal/vertical steel bars, (b)(e) RANASC fit image X–Z Perspective, (c)(f) BSFM-RANASC fit image X–Z Perspective.

Table 4. Comparison of measurement radii for steel bars.

Rebar	Actual rebar diameter(R)	$A(\hat{R})$	Average error	Average error rate
Rebar1	0.03600	0.03663	0.00063	1.7%
Rebar2	0.03600	0.03645	0.00045	1.2%

distribution of the point cloud is non-uniform due to sampling angle constraints, with a dense primary diagonal and sparse sides. The point cloud segments of the horizontal and vertical rebars extracted from Fig. 10(c) were processed using both the conventional RANSAC and the optimized algorithm proposed in this study. For a fair comparison, we set the iteration count for both algorithms to 5,000. The initial threshold for RANSAC was set at the actual radius of the rebar, 0.03600 m. Comparative images are presented in Fig. 11.

Evaluation metric: Given the horizontal orientation of the rebar mesh, with both vertical rebars forming a 90° angle with the ground and horizontal rebars perpendicular to the vertical plane, our precision evaluation metric is the error in the angle between the fitted lines from both the RANSAC and BSFM-RANSAC algorithms and their respective vertical planes. The formula for calculating this angle between the line and the plane is as follows:

$$\theta = \arctan\frac{AA'}{BA'} = \arctan\frac{\sqrt{(x_2-x_1)^2+(y_2-y_1)^2}}{|z_1-z_2|}. \quad (11)$$

In order to evaluate the performance of the developed algorithm, the relevant parameters:line-plane pinch angle Z and rebar radius R are estimated. The estimated line-plane pinch angle $A(\hat{Z})$ and the estimated rebar radius $A(\hat{R})$ are calculated according to definition in Eq. (12):

$$\begin{aligned} A(\hat{Z}) &= \frac{1}{S}\sum_{i=1}^{S}|\hat{Z}_i, \\ A(\hat{R}) &= \frac{1}{S}\sum_{i=1}^{S}|\hat{R}_i, \end{aligned} \quad (12)$$

where $\hat{Z}_i$ and $\hat{R}_i$ are the estimated line-plane angle and radius of the i sample, respectively, and S is the number of samples, which is set to 10 herein addition, the errors of different algorithm fits are compared using the mean-square error (MSE) of the line-plane angle Z, defined as

$$\mathrm{MSE}(\hat{Z}) = \frac{1}{S}\sum_{i=1}^{S}|Z_i \hat{-} Z|^2. \quad (13)$$

The experimental results are shown in Table 3, and the performance of BSFM-RANSAC's calculation results is significantly better than that of RANSAC, with higher geometric restoration in real projects. In addition, the error threshold (rebar radius) of RANSAC is set manually, and BSFM-RANSAC automatically calculates the optimal threshold through the scoring function, the calculation results are shown in Table 4, and the error of the rebar radius detection is not more than 2%.

4.3.2. *Line fitting of multiple steel bars*

The sequential RANSAC framework consists of successively applying the standard RANSAC model and then removing the detected outliers. However, in the case of high noise, some crossover models may have more interior regions than the true model [18], as shown in Fig. 12.

In this paper, the RANSAC algorithm and the improved algorithm are used to fit the multiple rebar line model, respectively, and the algorithm process is as follows: the RANSAC manually inputted the rebar radius as an error threshold, and the BSFM-RANSAC algorithm automatically estimated it, and the number of iterations were all set to 5000. Initially, a single rebar was fitted. Starting from the second iteration, the optimal rebar model was extracted from the dataset excluding the scan points of the line detected in the previous iteration. This process was

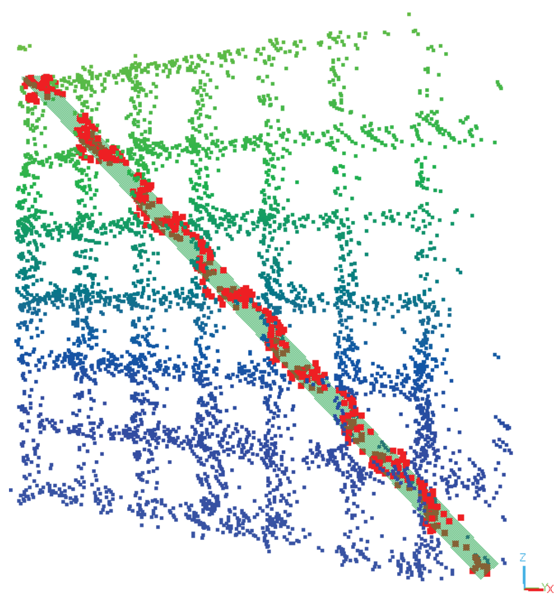

Fig. 12. Severe distortion of line fitting caused by high noise. And RANSAC wrongly fitted a line to do an incorrect prediction.

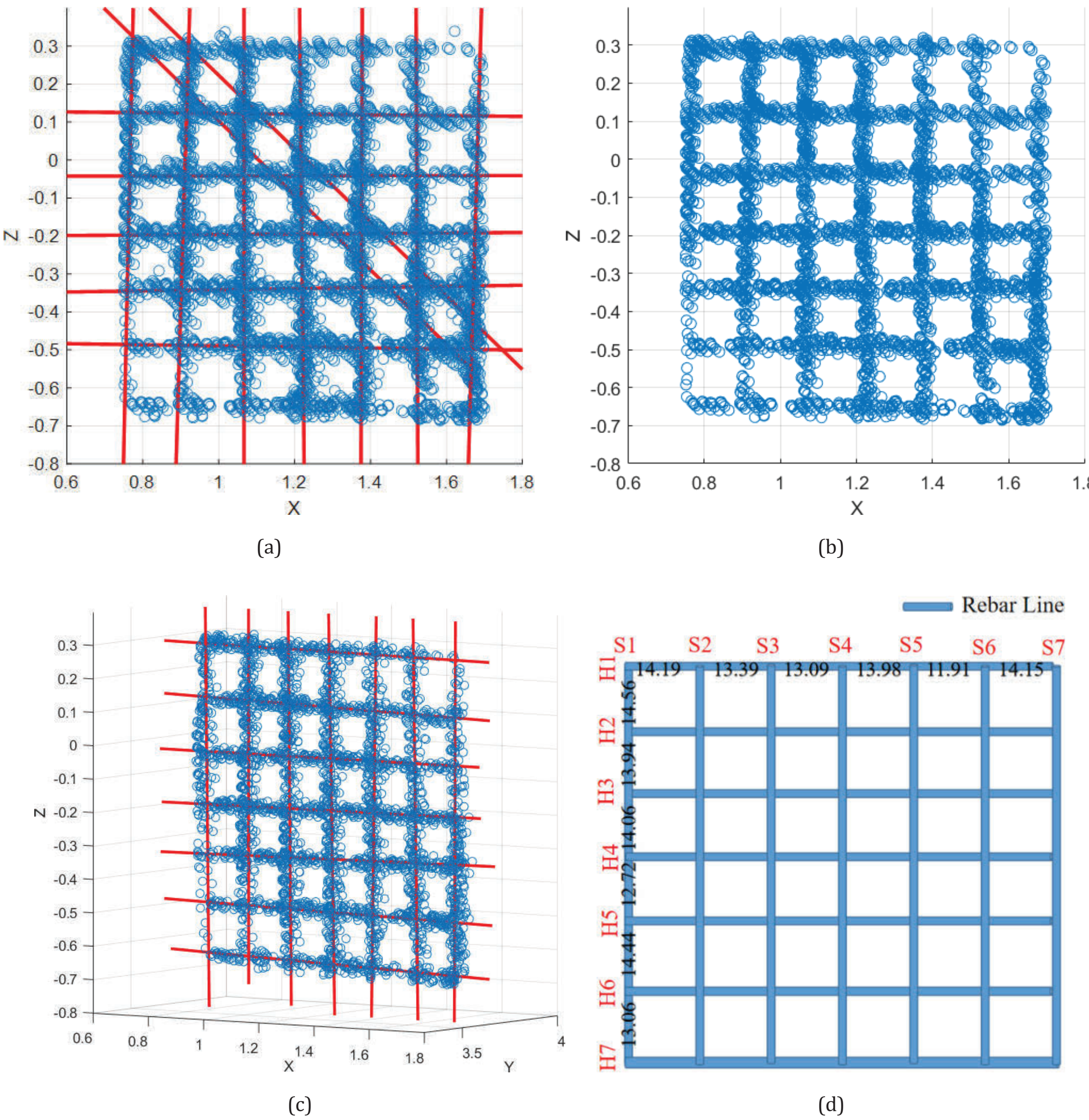

Fig. 13. Results. (a) RANSAC multiple model wrongly fitting *X–Z* perspective, (b) BSFM-RANSAC multiple correct dense model fitting *X–Z* perspective, (c) BSFM-RANSAC multiple extracted model fitting results, (d) Measurement value of steel bar spacing.

Table 5. Assessment of steel bar spacing accuracy.

Rebar type	Rebar number	Actual spacing	Measure spacing	Average error	Accuracy
Horizontal	H1–H2	0.15183	0.1456	0.00623	95.90%
Horizontal	H2–H3	0.14028	0.1394	0.00088	98.17%
Horizontal	H3–H4	0.13908	0.1406	0.00152	98.92%
Horizontal	H4–H5	0.12726	0.1272	0.00006	99.95%
Horizontal	H5–H6	0.13710	0.1444	0.00730	94.94%
Horizontal	H6–H7	0.13744	0.1306	0.00684	95.02%
Vertical	S1–S2	0.14013	0.1419	0.00177	98.75%
Vertical	S2–S3	0.12859	0.1339	0.00531	96.03%
Vertical	S3–S4	0.12876	0.1309	0.00214	98.37%
Vertical	S4–S5	0.14390	0.1398	0.00410	97.15%
Vertical	S5–S6	0.12868	0.1191	0.00958	92.56%
Vertical	S6–S7	0.14638	0.1415	0.00488	96.67%

repeated iteratively until the rebar model score fell below the threshold inlier count or the threshold score $S's$. The final comparison of the results is illustrated in Fig. 13.

The experimental results in Fig. 13 show that RANSAC performs inadequately on the given dataset and is prone to detecting cross-models, which significantly disrupts the overall structure of the reinforcing mesh. In contrast, the BSFM-RANSAC algorithm, with its bi-objective scoring function, effectively avoids the generation of cross-models, resulting in final fitting outcomes that accurately reflect the real-world scenario. The multi-model fitting accuracy ratings are provided in Table 5.

Rebar spacing measurement is a crucial metric for the practical three-dimensional reconstruction of rebar mesh [19]. To reduce randomness, the spacing measurements reported here were averaged over 10 trials for each dataset. The results indicate that the average accuracy for both horizontal and vertical rebar models exceeds 95%, demonstrating the feasibility and precision of the proposed optimization algorithm.

5. Conclusion

This paper presents a formalized and improved RANSAC fitting method, which was inspired by an autonomous spray robot scenario in the field of automation in construction. The accurate determination of inliers, particularly at the boundary with external points, poses a significant challenge. To address this challenge, the proposed BSFM-RANSAC model fitting method aims to clarify the delineation between different zones or entities within the dataset. The experimental results demonstrate that the proposed method outperforms the other three classical methods in terms of fitting accuracy and robustness in both 2D and 3D fitting tasks. It effectively captures the geometry of reinforcing meshes during real reinforcing mesh inspections. In future research, we plan to improve the efficiency of the optimization algorithm by addressing its computational speed limitations. Additionally, we aim to expand its applicability to the detection of various types of morphologies, such as circles, spheres, ellipses, and others, within real systems.

Acknowledgments

This work was supported by the China Three Gorges Corporation under Award Number WWKY-2021-0483. It is additionally supported by the National Natural Science Foundation of China under Award Number 51408069.

ORCID

Fengling Li https://orcid.org/0009-0009-2179-2936
Zhengan Yin https://orcid.org/0009-0001-1674-1319
Xiangqian Li https://orcid.org/0000-0001-6127-5209
Junfeng Zhang https://orcid.org/0009-0003-1548-2348

References

[1] H. Ahmed, H. M. La and K. Tran, Rebar detection and localization for bridge deck inspection and evaluation using deep residual networks, *Autom. Constr.* **120** (2020) 103393.
[2] M. Fan, S.-W. Jung and S.-J. Ko, Highly accurate scale estimation from multiple keyframes using ransac plane fitting with a novel scoring method, *IEEE Trans. Vehicular Tech.* **69**(12) (2020) 15335–15345.
[3] B. Wang, Z. Zhao, Y. Chen and J. Yu, A novel robust point cloud fitting algorithm based on nonlinear gauss–helmert model, *IEEE Trans. Instrum. Meas.* **72** (2023) 1–12.
[4] Q. Wu, J. Liu, C. Gao, B. Wang, G. Shen and Z. Li, Improved ransac point cloud spherical target detection and parameter estimation method based on principal curvature constraint, *Sensors* **22**(15) (2022) 5850.
[5] Z. Xie, G. Zhu, D. Zhang, D. Peng, J. Hu and Y. Sun, Line-features-based pose estimation method for the disc cutter holder of shield machine, *Sensors* **23**(3) (2023) 1536.
[6] M. A. Fischler and R. C. Bolles, Random sample consensus: A paradigm for model fitting with applications to image analysis and automated cartography, *Commun. ACM* **24**(6) (1981) 381–395.
[7] C.-M. Cheng and S.-H. Lai, A consensus sampling technique for fast and robust model fitting, *Pattern Recognit.* **42**(7) (2009) 1318–1329.
[8] J. Matas, O. Chum, M. Urban and T. Pajdla, Robust wide-baseline stereo from maximally stable extremal regions, *Image Vis. Comput.* **22**(10) (2004) 761–767.
[9] O. Chum and J. Matas, Matching with prosac-progressive sample consensus, in *2005 IEEE Computer Society Conf. Computer Vision and Pattern Recognition (CVPR'05)*, (IEEE, 2005), pp. 220–226.
[10] D. Barath, J. Noskova, M. Ivashechkin and J. Matas, Magsac++, a fast, reliable and accurate robust estimator, in *Proc. IEEE/CVF Conf. Computer Vision and Pattern Recognition*, (IEEE, 2020), pp. 1304–1312.
[11] P. H. Torr and A. Zisserman, Mlesac: A new robust estimator with application to estimating image geometry, *Comput. Vis. Image Understanding* **78**(1) (2000) 138–156.
[12] R. Raguram, J.-M. Frahm and M. Pollefeys, A comparative analysis of ransac techniques leading to adaptive real-time random sample consensus, in *Computer Vision–ECCV 2008: 10th European Conf. Computer Vision*, Marseille, France, October 12–18, 2008, Proceedings, Part II (Springer, 2008), pp. 500–513.
[13] L. Moisan, P. Moulon and P. Monasse, Automatic homographic registration of a pair of images, with a contrario elimination of outliers, *Image Processing On Line* **2** (2012) 56–73.
[14] Q. Wang, J. C. Cheng and H. Sohn, Automated estimation of reinforced precast concrete rebar positions using colored laser scan data, *Comput.-Aided Civ. Inf. Eng.* **32**(9) (2017) 787–802.
[15] D. Barath, J. Noskova and J. Matas, Marginalizing sample consensus, *IEEE Trans. Pattern Anal. Mach. Intell.* **44**(11) (2021) 8420–8432.
[16] C. V. Stewart, Minpran: A new robust estimator for computer vision, *IEEE Trans. Pattern Anal. Mach. Intell.* **17**(10) (1995) 925–938.

[17] P. H. Torr and D. W. Murray, Outlier detection and motion segmentation, in *Sensor Fusion VI*, Vol. 2059 (SPIE, 1993), pp. 432–443.
[18] H. Isack and Y. Boykov, Energy-based geometric multi-model fitting, *Int. J. Comput. Vis.* **97**(2) (2012) 123–147.
[19] M.-K. Kim, J. P. P. Thedja and Q. Wang, Automated dimensional quality assessment for formwork and rebar of reinforced concrete components using 3d point cloud data, *Autom. Constr.* **112** (2020) 103077.

Fengling Li is Associate Professor in Changsha University of Science & Technology, China. She received the M.S. and Ph.D. degrees in control theory and control engineering from Central South University, China, in 1998 and 2009. From 2002 to 2004, she was Lecturer in Changsha University of Science & Technology, China. Her scientific interests include intelligent instrument, robot perception and robot planning algorithm. She is the Director of Hunan Instrument Association.

Xiangqian Li received his Ph.D. degree in Geological Engineering from the China University of Geosciences, Beijing, in 2020. He is currently a senior engineer at the Science and Technology Research Institute of China Three Gorges Corporation, responsible for research on digital technology in hydropower engineering.

Zhengan Yin received a Bachelor's degree in Measurement and Control and Technical Instruments from Changsha University of Science & Technology in 2017 and is currently pursuing a Master's degree in Mechatronics at Changsha University of Science & Technology. The main research directions include tunnel 3D reconstruction, laser point cloud processing, and industrial robot trajectory planning.

Junfeng Zhang received his B.S. degree in Mechanical and Electronic Engineering from Changsha University, in 2021 and is currently pursuing a Master's degree in Mechanical major at School of Automotive and Mechanical Engineering, Changsha University of Science and Technology. His research interests are unsupervised location and identification of tunnel irregular rebar mesh and trajectory planning of tunnel shotcrete robots.